Communication

A Slot Antenna Array With Reconfigurable RCS Using Liquid Absorber

Yukun Zou, Xiangkun Kong, Lei Xing, Shunliu Jiang, Xuemeng Wang, He Wang, Zhiming Liu, Yongjiu Zhao, and Jens Bornemann

***Abstract*— A method is presented to achieve a slot antenna array with a reconfigurable radar cross section (RCS) by injecting and extracting ethanol. In a complex communication system, this can be used to switch between the detection and stealth modes. The antenna system is formed by combining a liquid absorber with a 2 × 2 slot antenna array. The liquid absorber consists of a polymethyl methacrylate (PMMA) container, 45% ethanol layer, and metal ground, which is attached to the surface of the slot antenna array. The incident wave can be absorbed by the absorber rather than reflected in other directions when the PMMA container is filled with ethanol, which reduces the monostatic and bistatic RCS. Thus, the RCS of the antenna can be changed by injecting and extracting ethanol while sustaining the antenna's radiation performance in terms of bandwidth, radiation patterns, and gain. The mechanism of the absorber is investigated. The simulated results show that the antenna with this absorber has monostatic and bistatic RCS reduction bands from 2.0 to 18.0 GHz and a maximum RCS reduction of 35 dB with an average RCS reduction of 13.28 dB. Without ethanol, the antenna realizes a gain of 12.1 dBi, which drops by 2 dB when the lossy ethanol is injected. The measured and simulated results agree well.**

***Index Terms*— Ethanol, radar cross section (RCS), reconfigurable, slot antenna array.**

I. Introduction

The radar cross section (RCS) is of fundamental importance in defense electronics, and related antennas usually contribute to good RCS values for stealth platforms [1]. In contrast with the RCS reduction of common objects, it is necessary in this scenario to maintain the radiation characteristics of antennas while achieving low scattering properties.

Recently, several approaches have been proposed to reduce the RCS of antennas. In these techniques, metasurfaces have been widely used, and metasurfaces with filtering features have been applied as excellent measures to reduce the RCS. For example, bandpass frequency-selective surfaces (FSSs) as radomes [2], [3] or a band-notched FSS as a metal ground [4], [5] were applied to reduce the out-of-band RCS of antennas. Another option is to load the antenna with metamaterial absorbers [6], [7]. In this way, the in-band and out-of-band RCSs will be reduced, but this method sometimes compromises the antenna gain. Furthermore, chessboard-layout metasurfaces were employed to reduce the antenna RCS through the phase cancellation between the incident and reflected waves [8]–[11].

This method can effectively reduce the in-band RCS. Moreover, polarization conversion metasurfaces were used to reduce the RCS of antennas [12]–[16]. This technology can achieve ultrawideband RCS reduction, but it is only effective for the monostatic RCS. An integrating design of antennas and low-scattering metasurfaces can achieve low-RCS systems, while the radiation characteristics are well maintained [17], [18]. The combination of Fabry–Perot (FP) resonator antennas and low-scattering metasurfaces is an excellent way to deal with gain reduction [19]–[22]. Specifically, combining a polarization conversion metasurface with a metamaterial absorber can achieve superior RCS reduction [23]. In this method, the in-band co-polarized waves will be transformed into their cross-polarized waves and then absorbed, whereas the out-of-band waves will be absorbed directly.

The low RCS antennas discussed above fall in the category of passive devices, which are mostly inflexible after fabrication. Unfortunately, switching and multifunction antennas are frequently required in practical applications due to changes in a real environment. To date, some liquid absorbers have been proposed for their wide absorption band, transparency, reconfigurable properties, low RCS, and low price of the liquid materials. A liquid material can be used as a radiator [24], [25], or it can be used as a unit cell to absorb incident waves [26]–[28].

To overcome the challenge of RCS reconfigurability, this study focuses on a three-layer liquid absorber to reduce the wideband RCS of a 2 × 2 slot antenna array. The liquid absorber can absorb incident waves, thereby reducing the RCS. The absorption band of the absorber ranges from 6.1 to 18 GHz. The simulated results show that the antenna equipped with this absorber exhibits monostatic and bistatic RCS reduction bands from 2.0 to 18.0 GHz and a maximum RCS reduction of 35 dB with an average RCS reduction of 13.28 dB. The reconfigurable property of the antenna is performed by injecting and extracting ethanol in a polymethyl methacrylate (PMMA) container. The mechanism and functionality of the liquid absorber are analyzed, and the RCS reconfigurable performance of the antenna is investigated. The novelty of our design lies in that a wide switchable absorption band can be achieved by leveraging the fluidity of the ethanol layer.

This communication is organized as follows. Section II introduces the geometry and mechanism of the absorber. Section III presents the radiation parameters and scattering properties of the low-RCS slot array antenna with an absorber, as well as the design and construction of the antenna. Finally, Section IV concludes the communication.

II. Design of the Absorber

A. Permittivity of 45% Ethanol

The liquid absorber consists of a PMMA container, 45% ethanol (55% water) layer, and metal ground. The permittivity of the 45% ethanol at radio frequency can be represented using the Debye

Manuscript received 13 August 2021; revised 2 December 2021; accepted 14 December 2021. Date of publication 5 January 2022; date of current version 26 July 2022. This work was supported in part by the National Natural Science Foundation of China under Grant 62071227, in part by the Natural Science Foundation of Jiangsu Province of China under Grant BK20201289, in part by the Open Research Program in China's State Key Laboratory of Millimeter Waves under Grant K202027, in part by the Fundamental Research Funds for the Central Universities under Grant xcxjh20210402, and in part by the Natural Sciences and Engineering Research Council (NSERC) of Canada. *(Corresponding author: Xiangkun Kong.)*

Yukun Zou, Xiangkun Kong, Lei Xing, Shunliu Jiang, Xuemeng Wang, He Wang, and Yongjiu Zhao are with the College of Electronic and Information Engineering, Nanjing University of Aeronautics and Astronautics, Nanjing 211106, China (e-mail: xkkong@nuaa.edu.cn).

Zhiming Liu is with the School of Information Engineering, Nanchang University, Nanchang 330031, China.

Jens Bornemann is with the Department of Electrical and Computer Engineering, University of Victoria, Victoria, BC V8W 2Y2, Canada.

Color versions of one or more figures in this communication are available at https://doi.org/10.1109/TAP.2021.3138525.

Digital Object Identifier 10.1109/TAP.2021.3138525

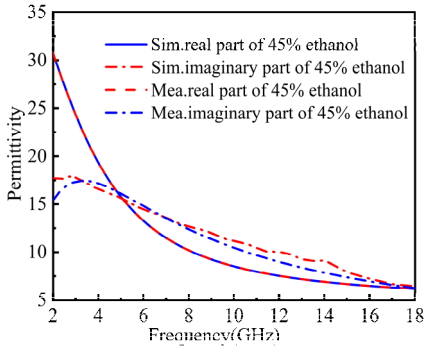

Fig. 1. Permittivity of 45% ethanol.

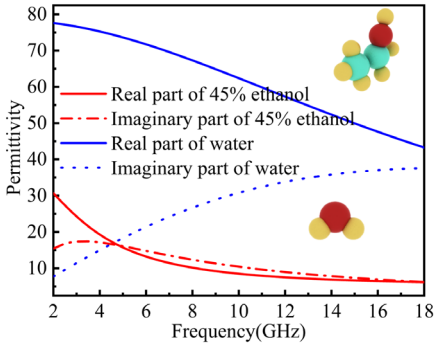

Fig. 2. Comparison of 45% ethanol and water.

formula with filled ethanol temperature T as follows [29]:

$$\varepsilon(\omega, T) = \varepsilon_\infty(T) + \frac{\varepsilon_0(T) - \varepsilon_\infty(T)}{1 - i\omega\tau(T)} \tag{1}$$

where $\varepsilon_\infty(\omega, T)$, $\varepsilon_0(T)$, and $\tau(T)$ are the optical permittivity, static permittivity, and rotational relaxation time, respectively. They are only related to temperature and can be expressed as

$$\varepsilon_0(T) = a_1 - b_1 T + c_1 T^2 - d_1 T^3 \tag{2}$$

$$\varepsilon_\infty(T) = \varepsilon_0(T) - a_2 e^{-b_2 T} \tag{3}$$

$$\tau(T) = c_2 e^{\frac{d_2}{T + T_0}} \tag{4}$$

where a_1, a_2, b_1, b_2, c_1, c_2, d_1, and d_2 are constant variables of ε0(T), $\varepsilon_\infty(T)$, and $\tau(T)$. Here, we set $T = 25$ °C, and hence, $\varepsilon(\omega, T)$ is only related to the frequency. First, the permittivity of 45% ethanol is measured by Dielectric Assessment Kit V 2.4 [30]. Then, the above equations are combined with the least-square method to fit the permittivity of the 45% ethanol. The fitting curves are in good agreement with the measured ones, as shown in Fig. 1. It can be seen that the imaginary part of the permittivity is large, which ensures that the liquid absorber has a good absorption property. The fitting curves of the permittivity will be applied to the full-wave electromagnetic simulation to obtain the features of the liquid absorber and the antenna array. The parameters are $\varepsilon_\infty(T) = 5.0344$, $\varepsilon_0(T) = 735.1702$, and $\tau(T) = 20.9273$.

The reason 45% ethanol is selected instead of all water or another percentage of ethanol is shown in Fig. 2. The real part of the permittivity of ethanol is substantially lower than that of water, thus allowing a thicker liquid layer, which enables us to make full use of the liquid's fluidity. It is necessary to point out that the real and imaginary parts of permittivity will be smaller with the increase in the ethanol percentage. Considering the fluidity of the liquid layer and the profile of the antenna, 45% ethanol is selected.

B. Structure of the Absorber

The proposed liquid absorber is a sandwich structure composed of a container layer, 45% ethanol layer, and metal ground, as shown in Fig. 3(a). The container is made of PMMA ($\varepsilon_r = 2.67$ and $\tan\delta = 0.01$) on the top layer, with square grooves that match the shape of the square-type ethanol, as shown in Fig. 3(b). With the metal ground, the container produces an enclosed chamber that will be filled with ethanol. The length and width of the PMMA container are $w_2 = 13$ mm, and its thickness is $h_2 = 9$ mm. The length and width of the square ethanol layer are $w_1 = 10$ mm, and its thickness is $h_1 = 5$ mm.

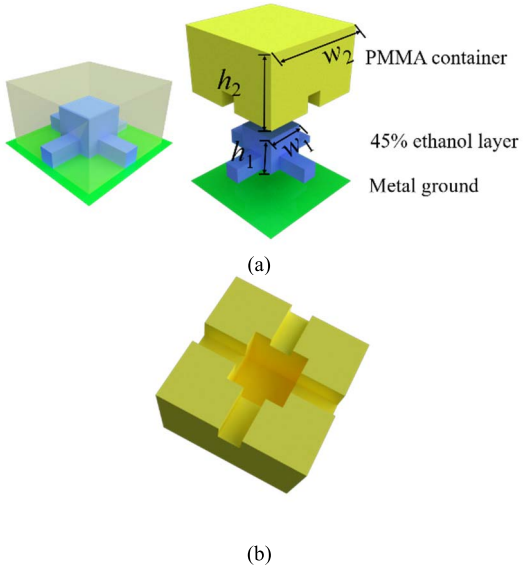

Fig. 3. (a) Unit cell structure of the absorber and (b) bottom view of the container.

Full-wave electromagnetic simulation is applied to examine S_{11} of the liquid absorber. The effects of different parameters on the absorption band are shown in Fig. 4. As shown in Fig. 4(a), as h_1 increases, the absorption band expands until it reaches $h_1 = 5$ mm, and then, the absorption band becomes narrower as h_1 continues to rise. Fig. 4(b) shows that as h_2 increases, the absorption band of the absorber remains nearly unchanged until $h_2 = 12$ mm, after which it narrows. The absorption band of the absorber changes slightly as w_1 changes, as shown in Fig. 4(c). In Fig. 4(d), it is observed that as w_2 increases, the property of the absorber deteriorates dramatically. The reason for the varied absorption band is that the impedance of the absorber does not match that of the free space due to its different parameter values. Finally, to obtain superior absorption properties of the absorber and better characteristics of the antenna, the optimized parameters are as follows: $h_1 = 5$ mm, $h_2 = 9$ mm, $w_1 = 10$ mm, and $w_2 = 13$ mm. The absorption band ($S_{11} < 10$ dB) of the absorber covers a frequency range of 6.1–18 GHz.

C. Mechanism of the Absorber

To better understand the mechanism of the absorber, we use a one-port network, as proposed in [31], to describe the impedance and S-parameters of the liquid absorber. For a parallel resonant circuit, the real part of the impedance is maximum and the imaginary part is minimum. Therefore, we can obtain the impedance of the absorber from the full-wave electromagnetic simulation; we find that there

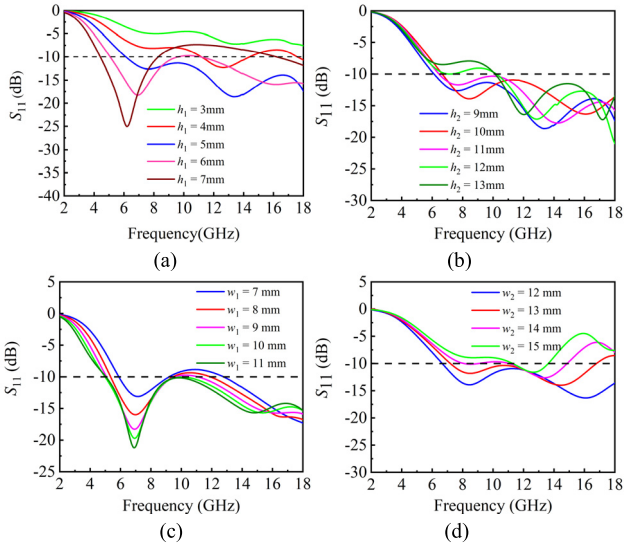

Fig. 4. S_{11} of the absorber with different values of (a) thickness of the ethanol layer h_1, (b) thickness of the container h_2, (c) width of the ethanol layer w_1, and (d) width of the container w_2.

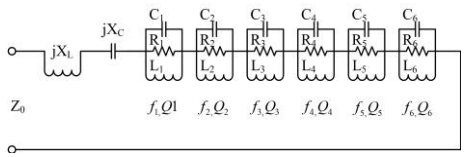

Fig. 5. Equivalent circuit model of the absorber.

are six maxima in the real part of the impedance. Thus, six parallel resonant circuits with resonant frequencies $f_1 - f_6$ and unloaded Q factors $Q_1 - Q_6$ are shown in Fig. 5. The series inductance and capacitance are described by $X_L(f) = X_{L0}f/f_c$ and $X_C(f) = X_{C0}f/f_c$, respectively, where f_c is the center frequency. In the circuit model, resonant frequencies, unloaded Q factors, and X_{L0} and X_{C0} can be found by a genetic algorithm. Thus, the impedance of the equivalent circuit model can be achieved and its S-parameters can be calculated by $Z = (1 + |S_{11}|)/(1 - |S_{11}|)$. The parameters are $Q_1 = 5.28$, $Q_2 = 4.38$, $Q_3 = 2.48$, $Q_4 = 2.52$, $Q_5 = 4.22$, $Q_6 = 4.01$, $f_1 = 4.28$ GHz, $f_2 = 4.72$ GHz, $f_3 = 5.68$ GHz, $f_4 = 11.39$ GHz, $f_5 = 15.5$ GHz, $f_6 = 20.95$ GHz, $X_{L0} = 141.2$ Ω, and $X_{C0} = 1.86$ Ω. The fitting results are shown in Fig. 6(a) and (b). The curves of impedance and S_{11} in ADS are slightly different from those in the full-wave electromagnetic simulation because the number of cascaded parallel resonant circuits is low. It is worth noting that the use of more cascaded parallel resonant circuits can achieve more accurate curves of the impedance and S_{11}.

The power-loss density of the absorption minima at 7.6, 13.3, and 17.7 GHz is presented in Fig. 7(a), (b), and (c), respectively. It is observed that at 7.6 GHz, the power is mainly concentrated on the top left and top right of the ethanol layer, the power is transferred to the upper surface of the ethanol layer at 13.3 GHz, and the majority of the power is localized at the interface of the ethanol layer and container layer at 17.7 GHz. This result reveals that the power is absorbed by the ethanol layer.

III. Design and Measurement of the Slot Antenna Array With Reconfigurable RCS

A. Antenna Structure

To verify the reconfigurable low-RCS function of the liquid absorber, we combine the absorber with a 2 × 2 slot antenna

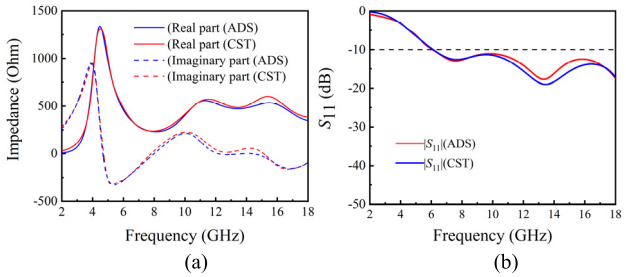

Fig. 6. (a) Comparison of impedance between ADS and CST. (b) Comparison of S_{11} between ADS and CST.

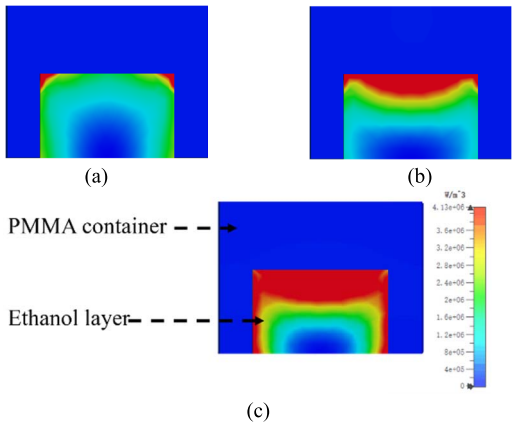

Fig. 7. Power-loss density. (a) $f = 7.6$ GHz. (b) $f = 13.3$ GHz. (c) $f = 17.7$ GHz.

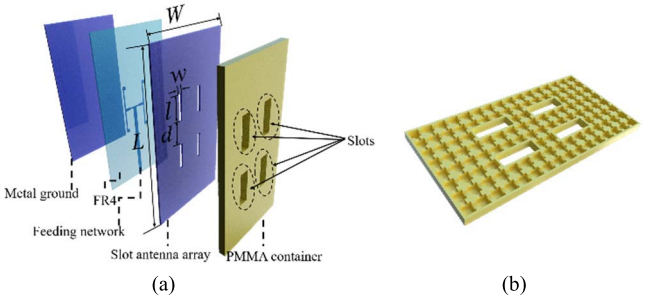

Fig. 8. (a) 3-D sketch of the antenna and (b) bottom view of the container.

array, as shown in Fig. 8(a). A metal ground with four slots is located on the top surface of a 1 mm-thick FR4 dielectric substrate ($\varepsilon_r = 4.4$ and $\tan\delta = 0.02$). W and L represent the width and length of the metal ground, respectively. The width and length of the slot are w and l, respectively, and the distance between slots is d. The feeding network is printed on the back of the FR4. A metal reflector is added to suppress the back lobe. The container with four slots is set on the surface of the metal ground, as shown in Fig. 8(a). The slots on the container are wider and longer than those on the metal ground, which can help the slot antenna array to maintain its radiation performance. A square space is adopted to contain the ethanol, and a slot is designed between the adjacent square spaces to ensure the fluidity of ethanol, as shown in Fig. 8(b). The parameters of the antenna are $W = 120$ mm, $L = 220$ mm, $w = 3$ mm, $l = 33.2$ mm, and $d = 30$ mm.

B. Simulated and Measured Radiation Performance

The antenna has been fabricated and measured to demonstrate the reliability of our simulations. The container structure is fabricated

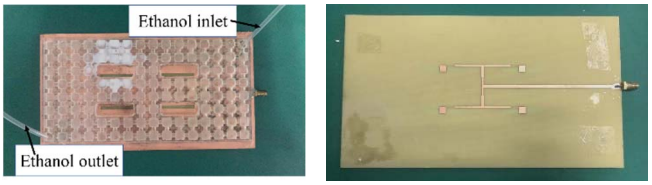

Fig. 9. Photographs of the fabricated (a) antenna and (b) feeding network of the antenna.

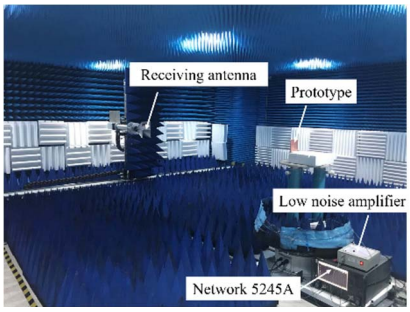

Fig. 10. Measurement setup of the radiation performance.

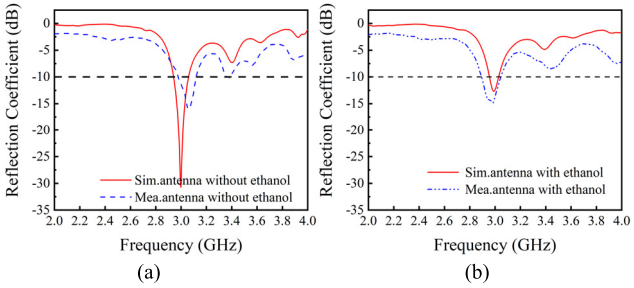

Fig. 11. Simulated and measured reflection coefficients of the antenna (a) without ethanol and (b) with ethanol.

by a numerically controlled machine tool and the slot antenna array is fabricated by the PCB process. Fig. 9(a) and (b) shows the photographs of the antenna and the feeding network. A 5245A vector network analyzer was used to measure the reflection coefficient, and the radiation patterns were measured in a microwave anechoic chamber, as shown in Fig. 10.

Fig. 11 presents the reflection coefficient of the antenna with or without ethanol. The 10 dB return-loss bandwidth of the antenna, with or without ethanol, is approximately 100 MHz, ranging from 2.94 to 3.04 GHz. The difference between simulation and measurement is attributed to the glass glue used to seal the ethanol, which slightly changes the impedance of the antenna. The simulated and measured radiation patterns of the antenna with and without ethanol at 3 GHz are shown in Fig. 12. The 3-D radiation patterns of the antenna with and without ethanol are shown in Fig. 13.

The radiation patterns reveal that the radiation performance of the antenna without or with ethanol remains nearly identical, which coincides with our initial hypothesis. The realized gain of the antenna without ethanol is 12.1 dBi at 3 GHz. As the layer is filled with ethanol, the gain drops by 2 dB due to ethanol loss. However, considering the good scattering property of the liquid absorber, this effect is acceptable. The simulated and measured gains of the antenna with and without ethanol are shown in Fig. 14. The glass glue and background noise are assumed to cause a small difference between the simulation and experimental results.

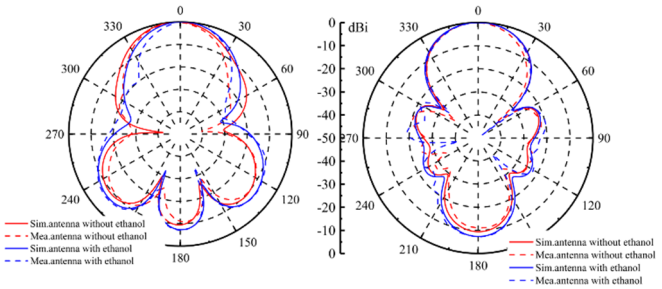

Fig. 12. Simulated and measured radiation patterns of the antenna with ethanol and without ethanol at 3 GHz. (a) *xoz* plane. (b) *yoz* plane.

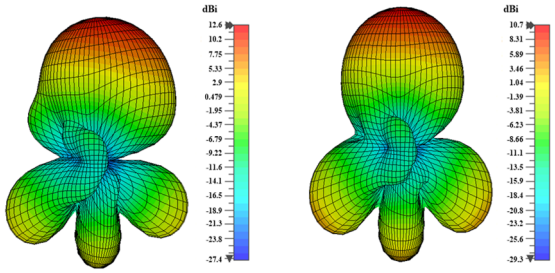

Fig. 13. 3-D radiation patterns of the antenna at 3 GHz: (a) without ethanol and (b) with ethanol.

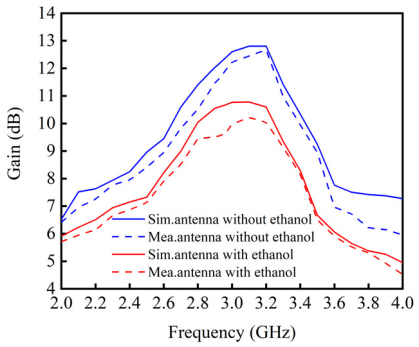

Fig. 14. Simulated and measured gains of the antenna with and without ethanol.

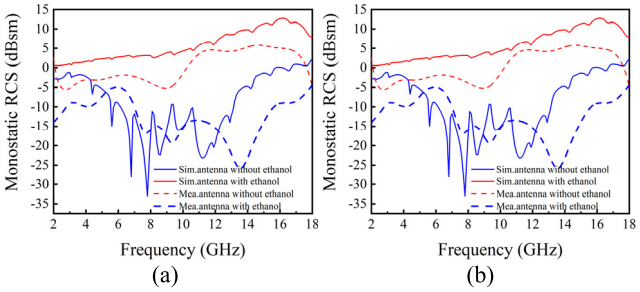

Fig. 15. Simulated and measured monostatic RCS of the antenna with and without ethanol. (a) x-polarized wave. (b) y-polarized wave.

C. Simulated and Measured Radiation Performance

Fig. 15(a) and (b) shows the monostatic RCS of the antenna with and without ethanol for x- and y-polarized waves. The measured results are in reasonable agreement with the simulations. The following factors contribute to the difference between measurement

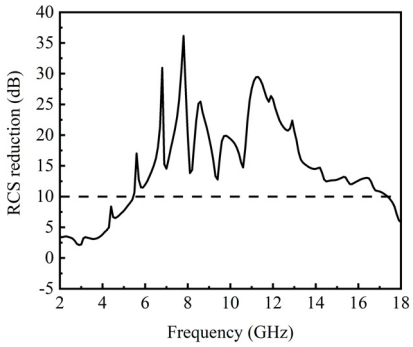

Fig. 16. RCS reduction of the antenna with ethanol compared with the antenna without ethanol.

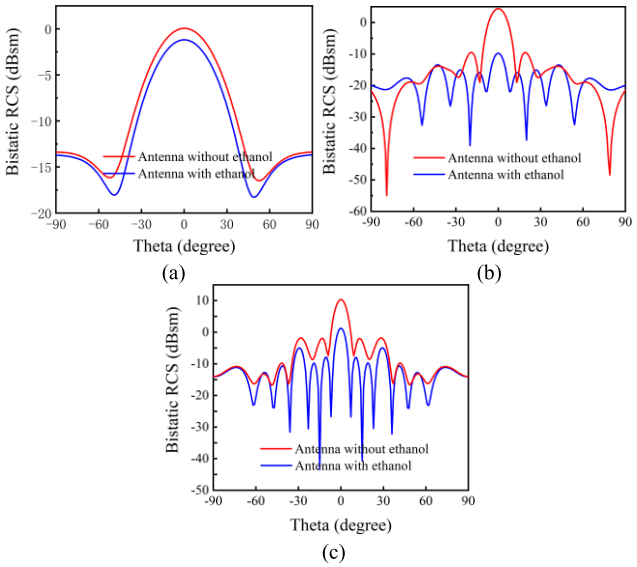

Fig. 17. Bistatic RCS of the antenna with and without ethanol at (a) 3, (b) 7.6, and (c) 16 GHz.

and experiment: 1) the impinging wave in the simulation is a plane wave, but the radiated wave of the standard horn antenna has a slightly spherical shape; 2) it is difficult to ensure that the container is completely filled with ethanol; 3) background noise in the measurement setup causes measurement tolerance; and 4) a small amount of misalignment is unavoidable in such a setup.

Fig. 16 shows the RCS reduction of the antenna with ethanol compared to the antenna without ethanol. It can be observed that the RCS decreases dramatically between 6 and 16 GHz because the absorber absorbs the majority of the power. In addition, from 2 to 6 GHz, the RCS of the antenna has a small reduction due to the influence of the container and the loss of the ethanol. The resonant frequency points are generated by the resonant cavity formed by the metal reflector and the slot antenna array. The maximum RCS reduction is 36 dB, and the average RCS reduction is 13.28 dB. Within the operating frequency band of the antenna, the bistatic RCS of the antenna with and without ethanol remains almost unchanged, and the slight difference between the two curves is caused by ethanol loss, as shown in Fig. 17(a). The bistatic RCS of the antenna is reduced obviously within the operation band of the absorber. This coincides with the operation band of the absorber and indicates that the absorber helps reduce the RCS of the antenna. In Fig. 17(b) and (c), we can see that the RCS increases in some directions because the absorber destroys the resonant pole. Fig. 18 shows the 3-D patterns of the RCS of the antenna with and without ethanol at 3, 7.6, and 16 GHz. It is found that the absorber

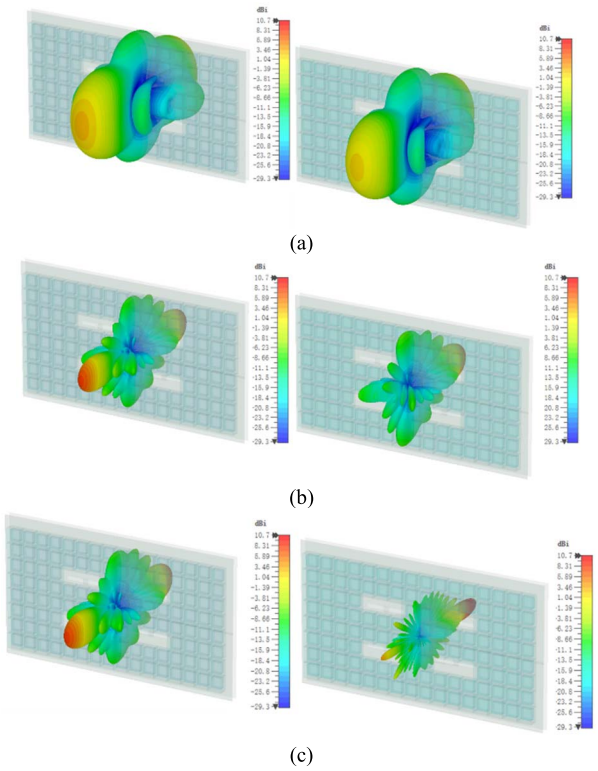

Fig. 18. 3-D patterns of RCS of the antenna with and without ethanol at (a) 3, (b) 7.6, (c) 16 GHz.

reduces the backward RCS, while the forward RCS of the antenna remains unchanged due to electromagnetic wave diffraction.

IV. Conclusion

This communication proposes a liquid-based reconfigurable RCS slot antenna array. A sandwich-structure liquid absorber with an absorption band ranging from 6.1 to 18 GHz was constructed by combining a 2×2 slot antenna array with an absorber, resulting in wideband monostatic RCS and bistatic RCS reduction. The RCS of the antenna can also be reconfigured by injecting and extracting ethanol while maintaining the radiation performance of the antenna, except for its gain, which is affected by the ethanol loss. The simulated and measured results show that the maximum monostatic RCS of the antenna with ethanol is 36 dB lower than that without ethanol at 6.7 GHz, and the bistatic RCS of the antenna with ethanol is 15 dB lower than that of the antenna without ethanol when $\theta = 0°$. This design could be applied in a stealth communication platform in the future.

References

[1] E. F. Knott, J. F. Shaeffer, and M. T. Tuley, *Radar Cross Section*. Raleigh, NC, USA: SciTech, 2004.
[2] F. Costa and A. Monorchio, "A frequency selective radome with wideband absorbing properties," *IEEE Trans. Antennas Propag.*, vol. 60, no. 6, pp. 2740–2747, Jun. 2012.
[3] L. Zhou and Z. Shen, "Hybrid frequency-selective rasorber with low-frequency diffusion and high-frequency absorption," *IEEE Trans. Antennas Propag.*, vol. 69, no. 3, pp. 1469–1476, Mar. 2021.
[4] Y. Han, L. Zhu, Y. Chang, and B. Li, "Dual-polarized bandpass and band-notched frequency-selective absorbers under multimode resonance," *IEEE Trans. Antennas Propag.*, vol. 66, no. 12, pp. 7449–7454, Dec. 2018.
[5] H. Huang, Z. Shen, and A. A. Omar, "3-D absorptive frequency selective reflector for antenna radar cross section reduction," *IEEE Trans. Antennas Propag.*, vol. 65, no. 11, pp. 5908–5917, Nov. 2017.

[6] T. Liu, X. Cao, J. Gao, Q. Zheng, W. Li, and H. Yang, "RCS reduction of waveguide slot antenna with metamaterial absorber," *IEEE Trans. Antennas Propag.*, vol. 61, no. 3, pp. 1479–1484, Mar. 2013.

[7] W. Li, X. Cao, J. Gao, Y. Zhao, and T. Liu, "A low RCS waveguide slot antenna array with metamaterial absorber," *IEEE Trans. Antennas Propag.*, early access, May 8, 2015, doi: 10.1109/TAP.2015.2431316.

[8] M. Paquay, J. C. Iriarte, I. Ederra, R. Gonzalo, and P. D. Maagt, "Thin AMC structure for radar cross-section reduction," *IEEE Trans. Antennas Propag.*, vol. 55, no. 12, pp. 3630–3638, Dec. 2007.

[9] J. C. I. Galarregui, A. T. Pereda, J. L. M. de Falcón, I. Ederra, R. Gonzalo, and P. de Maagt, "Broadband radar cross-section reduction using AMC technology," *IEEE Trans. Antennas Propag.*, vol. 61, no. 12, pp. 6136–6143, Dec. 2013.

[10] Y. Fu, Y. Li, and N. Yuan, "Wideband compsite AMC surfaces for RCS reduction," *Microw. Opt. Technol. Lett.*, vol. 55, no. 11, pp. 2562–2568, 2013.

[11] D. Sang, Q. Chen, L. Ding, M. Guo, and Y. Fu, "Design of checkerboard AMC structure for wideband RCS reduction," *IEEE Trans. Antennas Propag.*, vol. 67, no. 4, pp. 2604–2612, Apr. 2019.

[12] Y. Liu, K. Li, Y. Jia, Y. Hao, S. Gong, and Y. J. Guo, "Wideband RCS reduction of a slot array antenna using polarization conversion metasurfaces," *IEEE Trans. Antennas Propag.*, vol. 64, no. 1, pp. 326–331, Jan. 2016.

[13] K. Li, Y. Liu, Y. Jia, and Y. J. Guo, "A circularly polarized high-gain antenna with low RCS over a wideband using chessboard polarization conversion metasurfaces," *IEEE Trans. Antennas Propag.*, vol. 65, no. 8, pp. 4288–4292, Aug. 2017.

[14] Y. Liu, Y. Hao, K. Li, and S. Gong, "Radar cross section reduction of a microstrip antenna based on polarization conversion metamaterial," *IEEE Antennas Wireless Propag. Lett.*, vol. 15, pp. 80–83, 2016.

[15] E. Ameri, S. H. Esmaeli, and S. H. Sedighy, "Ultra wideband radar cross section reduction by using polarization conversion metasurfaces," *Sci. Rep.*, vol. 9, no. 1, pp. 1–8, Dec. 2019.

[16] X. Kong *et al.*, "A metasurface composed of 3-bit coding linear polarization conversion elements and its application to RCS reduction of patch antenna," *Sci. Rep.*, vol. 10, no. 1, pp. 1–10, Dec. 2020.

[17] Y. Han, L. Zhu, Y. Bo, W. Che, and B. Li, "Novel low-RCS circularly polarized antenna arrays via frequency-selective absorber," *IEEE Trans. Antennas Propag.*, vol. 68, no. 1, pp. 287–296, Jan. 2020.

[18] H. Yang *et al.*, "Low in-band-RCS antennas based on anisotropic metasurface using a novel integration method," *IEEE Trans. Antennas Propag.*, vol. 69, no. 3, pp. 1239–1248, Mar. 2021.

[19] S. Zarbakhsh, M. Akbari, F. Samadi, and A. Sebak, "Broadband and high-gain circularly-polarized antenna with low RCS," *IEEE Trans. Antenn. Propag.*, vol. 67, no. 1, pp. 16–23, Jan. 2019.

[20] L. Zhang *et al.*, "Realization of low scattering for a high-gain Fabry–Pérot antenna using coding metasurface," *IEEE Trans. Antennas Propag.*, vol. 65, no. 7, pp. 3374–3383, Jul. 2017.

[21] Y. Zheng *et al.*, "Wideband gain enhancement and RCS reduction of Fabry–Pérot resonator antenna with chessboard arranged metamaterial superstrate," *IEEE Trans. Antennas Propag.*, vol. 66, no. 2, pp. 590–599, Feb. 2018.

[22] Z. Liu, S. Liu, X. Zhao, X. Kong, Z. Huang, and B. Bian, "Wideband gain enhancement and RCS reduction of Fabry–Pérot antenna using hybrid reflection method," *IEEE Trans. Antennas Propag.*, vol. 68, no. 9, pp. 6497–6505, Sep. 2020.

[23] Y. Liu, Y. Jia, W. Zhang, and F. Li, "Wideband RCS reduction of a slot array antenna using a hybrid metasurface," *IEEE Trans. Antennas Propag.*, vol. 68, no. 5, pp. 3644–3652, May 2020.

[24] L. Xing, Y. Huang, S. S. Alja'Afreh, and S. J. Boyes, "A monopole water antenna," in *Proc. Loughborough Antennas Propag. Conf. (LAPC)*, Nov. 2012, pp. 7–10.

[25] Z. Hu, S. Wang, Z. Shen, and W. Wu, "Broadband polarization-reconfigurable water spiral antenna of low profile," *IEEE Antennas Wireless Propag. Lett.*, vol. 16, pp. 1377–1380, 2017.

[26] X. Yan *et al.*, "Water-based reconfigurable frequency selective rasorber with thermally tunable absorption band," *IEEE Trans. Antennas Propag.*, vol. 68, no. 8, pp. 6162–6171, Aug. 2020.

[27] Y. Shen, J. Zhang, Y. Pang, J. Wang, H. Ma, and S. Qu, "Transparent broadband metamaterial absorber enhanced by water-substrate incorporation," *Opt. Exp.*, vol. 26, no. 12, pp. 15665–15674, 2018.

[28] Y. Pang *et al.*, "Thermally tunable water-substrate broadband metamaterial absorbers," *Appl. Phys. Lett.*, vol. 110, no. 10, Mar. 2017, Art. no. 104103.

[29] A. Andryieuski, S. M. Kuznetsova, S. V. Zhukovsky, Y. S. Kivshar, and A. V. Lavrinenko, "Water: Promising opportunities for tunable all-dielectric electromagnetic metamaterials," *Sci. Rep.*, vol. 5, no. 1, p. 13535, Oct. 2015.

[30] *Dielectric Assessment Resources*. Accessed: Aug. 7, 2018. [Online]. Available: https://speag.swiss/products-zh-cmn/dak-zh-cmn/dak-probes-zh-cmn

[31] Y.-F. Ruan, Y.-X. Guo, and X.-Q. Shi, "Equivalent circuit model of a tri-resonance wideband dielectric resonator antenna," *Microw. Opt. Technol. Lett.*, vol. 55, no. 11, pp. 2562–2568, 2013.